Fundamental Investigation on Indoor Local 5G Radio Map Generation Using Real-time Spectrum Monitor for Realizing Smart Factory

Tatsuya Hatagi, Masataka Miyake, Suguru Kameda
Research Institute for Semiconductor Engineering (RISE), Hiroshima University
1–4–2 Kagamiyama, Higashi-Hiroshima 739–8527, Japan
Email: {hatagi-tatsuya, masataka-miyake, kameda3}@hiroshima-u.ac.jp

***Abstract*— In recent years, the demand for smart factories capable of wirelessly transmitting information and power has grown. Understanding the wireless environment within these factories is crucial for this transmission. As a fundamental investigation, we generated a radio map for the local fifth generation (L5G) using the 4.8-GHz band. This map was generated using the free-space propagation loss formula and the directivity measurement results of the transmitting antenna. We then measured the received power at four locations using a spectrum monitor. By comparing the radio map with these measurements, we found that it is possible to estimate the received power in the line-of-sight environments.**

***Index Terms*—radio map, smart factory, spectrum monitor, local fifth generation**

I. Introduction

In recent years, the realization of smart factories [1] that utilize technologies such as artificial intelligence (AI) and Internet of things (IoT) has been desired. In traditional production sites, information and power are transmitted by wires mainly from the perspective of reliability. In contrast, in smart factories, information and power are transmitted wirelessly to facilitate layout changes within the factory and to employ automated guided robots. In order to transmit information and power wirelessly, it is necessary to understand the wireless environment in the factory. Fig. 1 shows how a smart factory is designed. The wireless environment and the manufacturing process within the factory are digitally replicated in cyberspace, creating a digital twin [2] that mirrors the real-world conditions. Subsequently, wireless resource allocation, wireless power transmission (WPT), and wireless information transmission (WIT) are then simulated in cyberspace based on the real-world information. Finally, the results of the cyberspace simulation are then reflected in the physical space. By estimating the wireless environment during power transmission, it is possible to prevent radio interference.

In this paper, for the ultimate goal of estimating the wireless environment within smart factories, we will investigate the characterization of this environment using mathematical formulations and generate a highly accurate radio map of the local fifth generation (L5G) using the 4.8-GHz band. Our future work includes refining these formulations and performing parameter tuning, which will be carried out using simultaneous multi-location measurements at different frequencies with spectrum monitors.

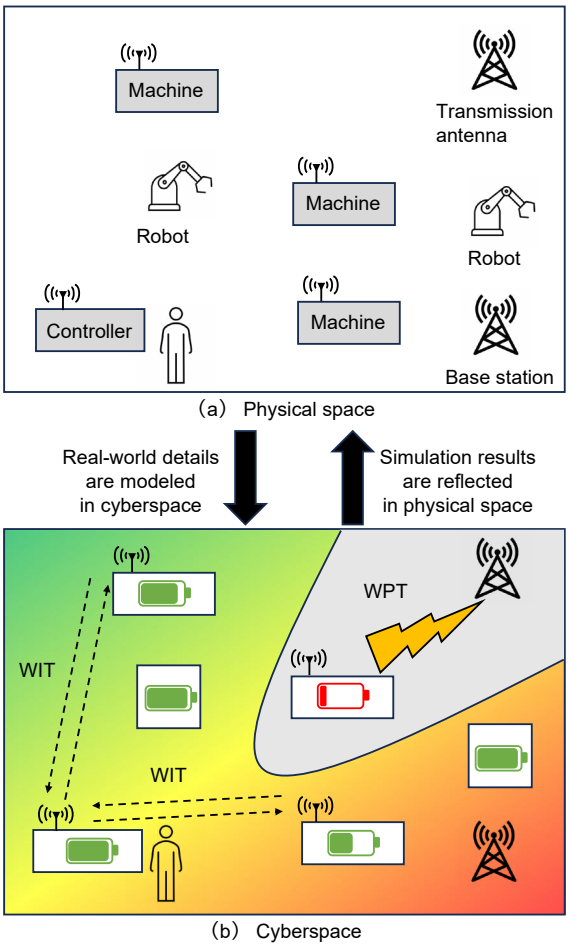

Fig. 1. Concept of smart factory. WPT, wireless power transmission; WIT, wireless information transmission.

The contents of this paper are as follows. In Sect. II, we modeled one-dimensional radio wave propagation profile based on the free-space propagation loss formula and the measurement results of the antenna directivity of the radio unit (RU) . In Sect. III, we measured the received power up to a distance of 14 m away from the origin, and confirmed that

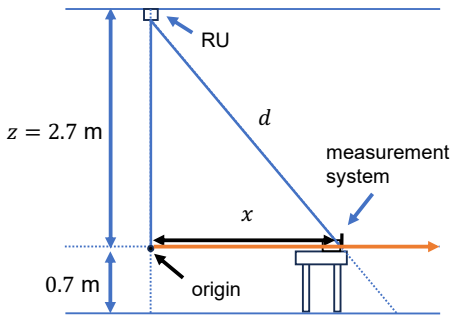

Fig. 2. Parameters for this calculation based on the measurement setup.

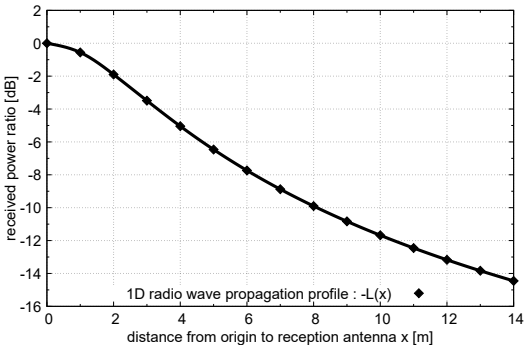

Fig. 3. Calculated one-dimensional radio wave propagation profile based on the measurement setup.

the one-dimensional radio wave propagation profile and the measurement results were approximately the same. In Sect. IV, we present how to generate the local 5G radio map and show the verification results of the radio map using the measured data of received power at four locations. Finally, in Sect. V, we conclude this paper.

II. One-dimensional Radio Wave Propagation Profile

A. Free-space propagation loss

In this section, one-dimensional radio wave propagation profile is modeled by the free-space propagation loss formula. Fig. 2 shows the parameters for this calculation based on the measurement setup. The origin is defined to be at the same height as the desk, directly below the RU. The x-axis was then set by the orange arrow from the origin. The distance from the origin to the reception antenna is denoted as x [m]. The distance between the origin and the RU is $z = 2.7$ [m]. The propagation distance between the antennas is denoted as $d = \sqrt{x^2 + z^2}$ [m], applying the Pythagorean theorem. According to the Friis transmission formula [3], the free-space propagation loss can be calculated by

$$L = 10 \log_{10}(4\pi d/\lambda)^2. \tag{1}$$

Eq. (1) is rewritten with x as

$$L(x) = 10 \log_{10} \left(4\pi \sqrt{x^2 + z^2}/\lambda\right)^2 \tag{2}$$

where the wavelength $\lambda = 6.181 \times 10^{-2}$ [m] corresponds to the center frequency $f = 4.850$ [GHz] of the L5G system used in this paper.

Based on the measurement setup, a one-dimensional radio wave propagation profile is calculated, as demonstrated in Fig. 3. Here, the negative value of $L(x)$ in Eq. (2) is plotted as a function of the distance x from 0 m to 14 m. The horizontal axis represents the distance x from the origin to the reception antenna. The vertical axis represents the received power ratio compared to the received power at the origin. The black line shows the results of the free-space propagation loss calculation. It is observed that the received power ratio decreases by 14.5 dB at the position 14 m away from the origin.

B. Directivity of the transmitting antenna (Experiment 1)

The environment in which radio waves propagate differs greatly between free space and the measurement environment. It is necessary to consider the effects of obstacles, reflections from metals, and the antenna directivity of both the transmission and reception antennas. In this subsection, the antenna directivity of the RU is examined. This is due to the fact that the angle of the reception antenna relative to the RU changes significantly depending on the reception antenna's position. As a result, the antenna gain of the RU also varies considerably. Therefore, we measured the antenna directivity of the RU (Experiment 1). This measurement was conducted on the third floor of the J-Innovation HUB building at the Research Institute for Semiconductor Engineering (RISE) Hiroshima University, where the RU of the L5G is installed. Fig. 4 shows the measurement environment for Experiment 1. The RU and the reception antenna were connected by a 2.5-m-long string so that the angle of the reception antenna relative to the RU could be changed while maintaining a constant distance. The angle of the reception antenna to the RU is donated as $\theta\,^\circ$, and the angle when the reception antenna is below the RU is defined as $0\,^\circ$. The received power was measured while increasing the angle θ. In the measurement, the reception antenna with a directivity of 37° at half-maximum width was used, and it was constantly directed towards the RU. The method for plotting the measured values was shown below. We extrapolated the line connecting the RU and the reception antenna. Then, we determined the length x from the origin to the intersection of this extrapolated line with the orange arrow. We obtained x by calculating $x = z \tan\theta$ and used this value when plotting the measured data in the next subsection.

Fig. 5 shows measurement results of the directivity of the RU. The horizontal axis represents the distance x from the origin to the reception antenna. The vertical axis represents the received power. The green plots shows the raw measurement data $P_{\mathrm{exp1,raw}}(x)$. The green line shows the approximate line $P_{\mathrm{exp1}}(x)$ derived from the raw data.

C. Proposed method

In this paper, we modeled the one-dimensional radio wave propagation profile by the free-space propagation loss formula

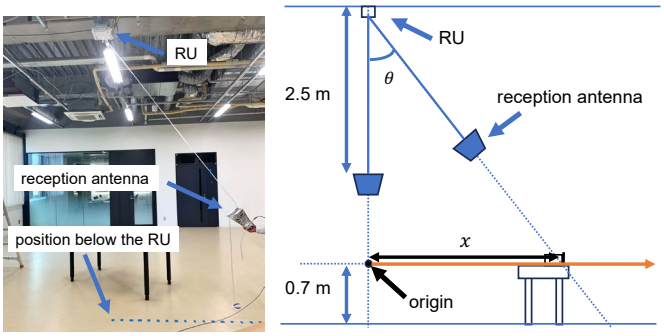

(a) Photograph (b) Diagram

Fig. 4. Measurement setup for Experiment 1.

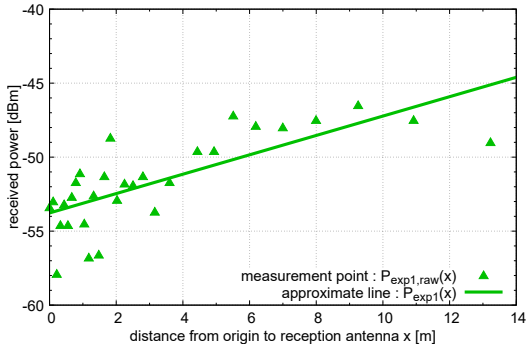

Fig. 5. Measurement results of the directivity of the RU, overlaid with its approximated line.

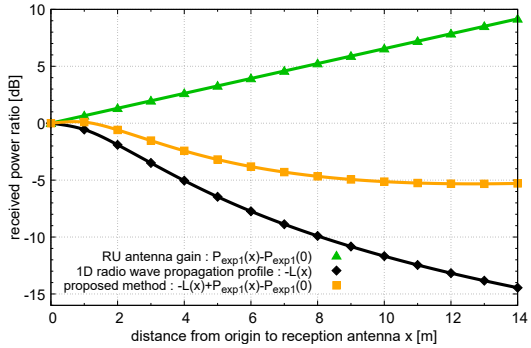

Fig. 6. Updated one-dimensional radio wave propagation profile with the antenna gain of the RU (shown with squares), overlaid with the antenna gain (with triangles) and with the plot in Fig. 5 (with diamonds).

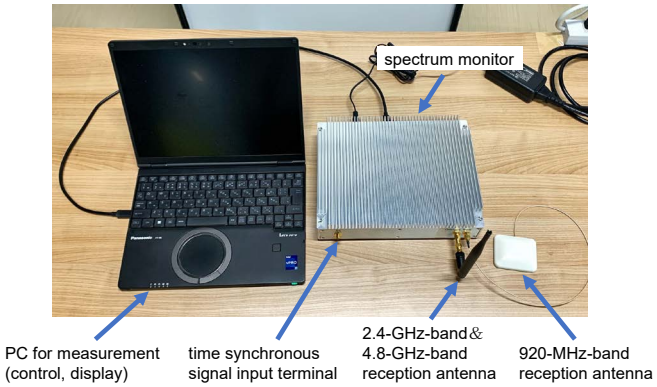

Fig. 7. Spectrum monitor with antennas and a PC.

and the measurement results of the antenna directivity of the RU. Fig. 6 shows the results of the free-space propagation loss calculation with correction by the antenna directivity of the RU. The horizontal axis represents the distance x from the origin to the reception antenna. The vertical axis represents the received power ratio compared to the received power at the origin. The green line shows the antenna gain of the RU, denoted as $P_{\mathrm{exp1}}(x) - P_{\mathrm{exp1}}(0)$. $P_{\mathrm{exp1}}(x)$ represents the received power at x, while $P_{\mathrm{exp1}}(0)$ corresponds to the received power at the origin, measured at -53.77 dBm. The black line shows the one-dimensional radio wave propagation profile denoted as $-L(x)$ shown in Subsect. II-A. The orange line shows the proposed method $-L(x) + P_{\mathrm{exp1}}(x) - P_{\mathrm{exp1}}(0)$. The results show that the antenna directivity of the RU had a significant effect on the one-dimensional radio wave propagation profile.

III. Verification Results in One-dimensional Profile

A. Overview of spectrum monitor

We aim to generate an indoor radio map, the accuracy of which can be enhanced through parameter tuning using the measurement results as a reference. This will be facilitated by spectrum monitors [4]–[6] that allow for simultaneous multi-location measurements even at different frequencies when their internal clocks are synchronized. In contrast, in this paper, we used the measurement results by the spectrum monitor as a reference for verification of the radio map. Fig. 7 shows the spectrum monitor used for Experiment 2 in Subsect. III-A and for Experiment 3 in Subsect. IV-B. The spectrum monitor is connected to a 920-MHz band reception antenna and a 2.4-GHz and 4.8-GHz band reception antenna. It can simultaneously measure the spectrum in the 920-MHz, 2.4-GHz, and 4.8-GHz bands. In this paper, the max-hold value displayed by the spectrum monitor was used as the received power. Spectrum monitors can be time-synchronized with a pulse per second (PPS) signal output from an external device such as a Global Positioning System (GPS).

B. Measurements of one-dimensional radio signal strength (Experiment 2)

Fig. 8 shows the measurement setup for Experiment 2. The RU was installed at a height of 3.4 m above the floor. The height of the desk was 0.7 m above the floor. Measurement points were placed at intervals of 0.1 m along a straight line up to 14 m from the origin. The measurement system shown in Fig. 7 was used in this experiment. The surrounding environment remained unchanged to conduct measurements in a quasi-stationary environment.

Fig. 9 shows the measurement results of Experiment 2. The horizontal axis represents the distance x from the origin to the reception antenna. The vertical axis represents the received

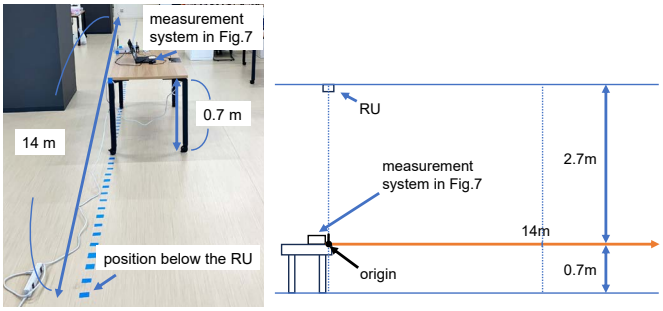

(a) Photograph (b) Diagram

Fig. 8. Measurement setup for Experiment 2.

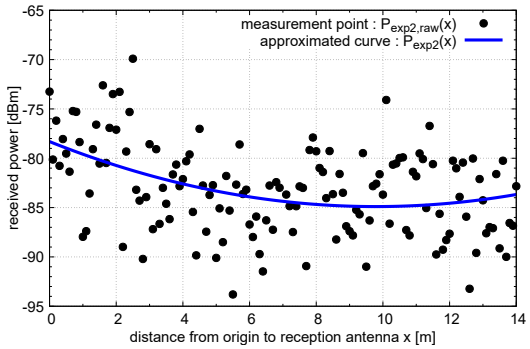

Fig. 9. Measured one-dimensional radio signal strength profile (Experiment 2), overlaid with its approximated curve.

power. The black plots indicate the raw measurement data $P_{\mathrm{exp2,raw}}(x)$. The blue line represents the approximate curve $P_{\mathrm{exp2}}(x)$, which was derived from the raw data using the method of least squares. It is observed that the magnitude of the variation of the raw data from the approximate curve was about 10 dB at its maximum. This is considered to be largely due to the effect of frequency-selective fading. The environment in which the measurements were conducted can be described as prone to reflection. This is because the ceiling and the walls are made of metal. In other words, it is considered that the spectrum monitor receives composite waves consisting of direct wave and multiple reflected waves, resulting in significant variations in received power regardless of the distance from the origin.

C. Verification of the proposed method

Fig. 10 shows the verification result of the proposed method (orange line) with the measurement results (blue line). The horizontal axis represents the distance x from the origin to the reception antenna. The vertical axis represents the received power ratio compared to the received power at the origin. The blue line shows the measured curve $P_{\mathrm{exp2}}(x) - P_{\mathrm{exp2}}(0)$ described in Subsect. III-A. The black line shows the one-dimensional radio wave propagation profile $-L(x)$ shown in Subsect. II-A. The orange line shows the proposed method $-L(x) + P_{\mathrm{exp1}}(x) - P_{\mathrm{exp1}}(0)$ described in Subsect. II-C. In the case of measurement results, the received power ratio

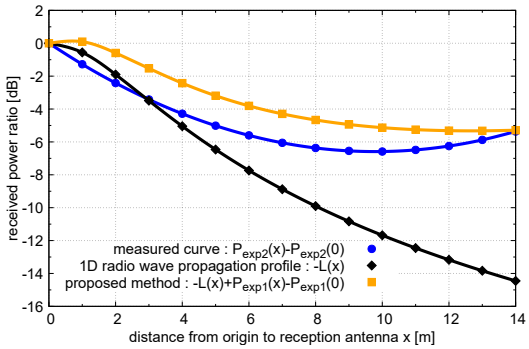

Fig. 10. Comparison between the measured curve in Fig. 9 (shown here by a line with dots) and the calculated result with the proposed method in Fig. 6 (with squares), also overlaid with the initial result in Fig. 5 (with diamonds).

compared to the received power at the origin decreases by 5.4 dB at a position 14 m away from the origin. On the other hand, in the case of the proposed method, it decreases by 5.3 dB, which is much better than 14.5 dB calculated only with the propagation loss described in Subsect. II-A. Therefore, it is confirmed that the proposed method and the measurement results are approximately the same.

IV. Extention to 2D Map

A. L5G radio map generation

Fig. 11 shows a floor map of the experiment site (the third floor of the J-Innovation HUB building at Research Institute for Semiconductor Engineering (RISE), Hiroshima University. The RU installation is represented by the gray square. The dimensions of the experiment site are 21.6 m in length and 25.8 m in width, while the area covered by the radio map are 16 m in length and 18 m in width. Certain sections of the experiment site were excluded from the radio map generation due to the presence of the anechoic chamber and the pillars. The dimensions of the pillar is 0.82 m in length and 0.92 m in width. The received power is calculated based on the proposed method as

$$P_{\mathrm{MAP}}(x) = P_{\mathrm{exp2,raw}}(0) - L(x) + P_{\mathrm{exp1}}(x) \qquad (3)$$

where $P_{\mathrm{exp2,raw}}(0)$ is the received power at the origin. It was measured to be -73.25 dBm in Experiment 2. In Eq. (3), by substituting x with r and incorporating the angle ϕ to utilize polar coordinates, the model can be extended to two dimensions, centered at the origin. Furthermore, by rotating ϕ through 360 degrees, a two-dimensional radio map based on Eq. (3) can be generated.

Fig. 12 presents the radio map, based on the proposed method, rendered on a grid with a resolution of 1 m^2. The RU of the L5G is installed at the open gray square. Black squares indicate pillars. The area enclosed by the blue line is the non line-of-sight due to either the pillars or the anechoic chamber. The color bar indicates the radio wave strength. As the value approaches the maximum, the shade of red becomes darker, while as it nears the minimum, the shade of green deepens. It is important to note that the radio map generated

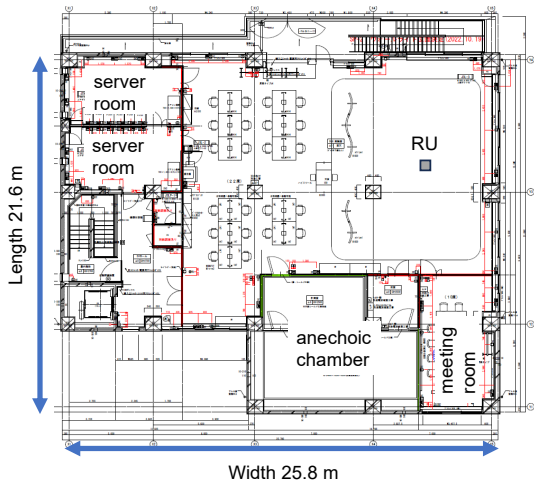

Fig. 11. Floor map of the experiment site (the third floor of the J-Innovation HUB, Hiroshima University).

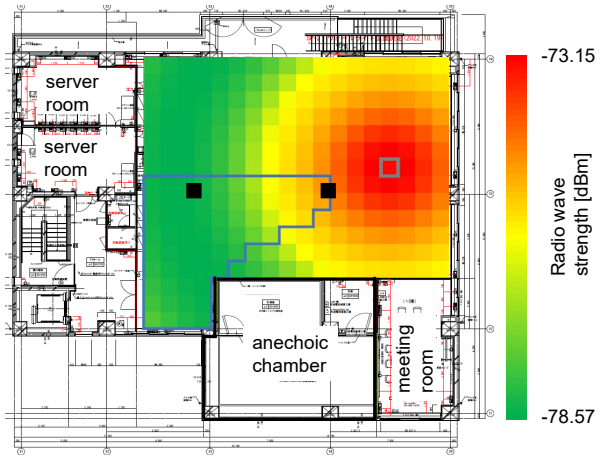

Fig. 12. L5G radio map generated with the extended proposed method. The open gray square represents the origin.

by this method assume that all locations are in the line-of-sight environments, however, in reality, there are locations that are in the non line-of-sight environment.

B. Verification with measured data (Experiment 3)

We measured the received power at the four locations shown with blue squares in Fig. 13 using a spectrum monitor (Experiment 3). The measurement locations are labeled as No. 1 to No. 4. No. 1, No. 3, and No. 4 are located in the line-of-sight environments, while No. 2 is located in the non-line-of-sight environment. We used the measurement system shown in Fig. 7. When measuring the received power, the operation status of the RU has to be considered. The L5G RU usually transmits signals using a part of the frequency band, and the transmission power constantly fluctuates. Therefore, in this measurement, we aimed to keep the transmission power of the RU constant by using a speed test in which the used bandwidth and the transmission power get at their maximum. The device conducting the speed test was positioned at the

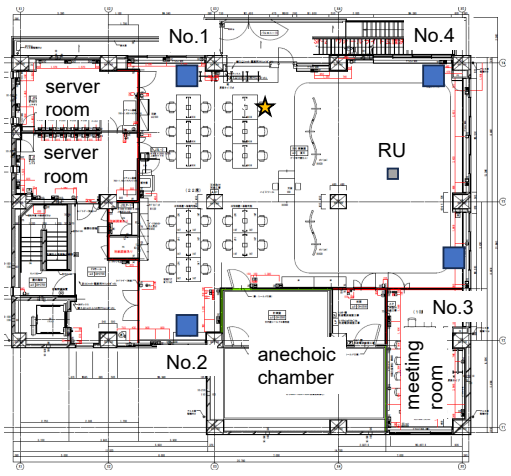

Fig. 13. Measurement setup for Experiment 3. The 4 squares show where the spectrum monitor (shown in Fig. 7) is placed.

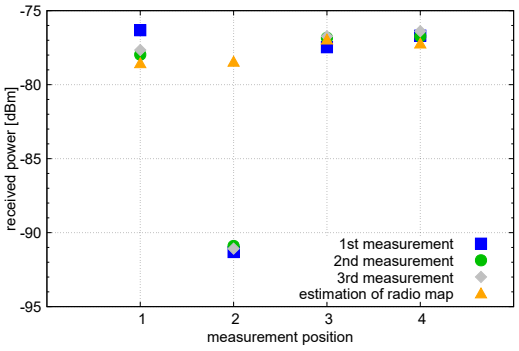

Fig. 14. Comparison of measurement results at each measurement location and estimated values from the radio map.

location indicated by the yellow star in Fig. 13. We used the downlink signals emitted from the RU during the speed test to measure the received power because they have a broader bandwidth that can mitigate the effects of fading.

Fig. 14 shows a comparison between the measured and estimated results for each measurement location. The blue, green, and gray plots represent the received power values at the first, second, and third measurement results respectively, while the orange plots represent the estimated received power values based on the radio map at each measurement location. The estimated received power in the non-line-of-sight environment (No. 2) showed an error of more than 10 dB compared to the actual measured received power. This discrepancy arose because the radio map assumes all locations are in the line-of-sight environments, whereas in reality, the pillars and the anechoic chamber obstructed direct wave reception, resulting in lower measured received power than estimated. In contrast, the error in the line-of-sight environments (No. 1, No. 3, and No. 4) was within 3.0 dB. In other words, it was found that the radio map generated by the proposed method can accurately estimate the received power in the line-of-sight environments.

V. Conclusions

This paper aims to generate a highly accurate radio map of the L5G using the 4.8-GHz band as a foundational study for modeling indoor wireless environment. The radio map was generated based on the free space propagation loss formula and the measurement results of the antenna directivity of the RU. As a result, the estimated received power in the line-of-sight environments showed an error of within 3.0 dB compared to the measured results. Conversely, in the non-line-of-sight case, the error was over 10 dB. From these results, it was found that in the line-of-sight environments, the proposed method allows for highly accurate estimation of received power.

ACKNOWLEDGEMENT

This paper is based on results obtained from a research project (No. JPJ012368C07301) commissioned by the National Institute of Information and Communications Technology (NICT). This work was carried out on the Local 5G Testbed at Hiroshima University which was deployed under the FY2022 National University Management Reform Promotion Project. The author would like to thank Mr. Nobumasa Arai for his cooperation in the measurement evaluation and data analysis.

References

[1] Ministry of Economy, Trade and Industry, The Cyber/Physical Security Guidelines for Factory Systems [Appendix: Key Considerations for Promoting Smartification], Apr. 2024.

[2] M. Grieves and J. Vickers, "Digital twin: Mitigating unpredictable, undesirable emergent behavior in complex systems," in Transdisciplinary Perspectives on Complex Systems: New Findings and Approaches, F.-J. Kahlen, S. Flumerfelt, and A. Alves Ed. Switzerland: Springer Cham, Aug. 2016, pp.85-113.

[3] H. T. Friis, "A note on a simple transmission formula," Proc. IRE and Waves and Electronics, pp.254-256, May 1946.

[4] T. Furuichi, M. Motoyoshi, S. Kameda, and N. Suematsu, "Direct RF under sampling receiver for wireless IoT real-time spectrum monitor using high-speed clock switching," SmartCom2018, IEICE Technical Report, vol.118, no.274, SR2018-68, pp. 21-24, Oct. 2018.

[5] T. Shiba, T. Furuichi, K. Akimoto, M. Motoyoshi, S. Kameda, and N. Suematsu "Real-time wideband spectrum monitor using multiple sampling frequency direct RF undersampling for wireless IoT," European Microwave Conference 2021 (EuMC2021), Feb. 2022.

[6] T. Furuichi, M. Motoyoshi, S. Kameda, T. Shiba, and N. Suematsu, "RF signal frequency identification in a direct RF undersampling multi-band real-time spectrum monitor for wireless IoT usage," IEICE Trans. Commun., vol.E105–B, no.4, pp. 461-471, Apr. 2022.